

Advances in Compatibility Assessment of Stainless Steels with Liquid Lead-Bismuth for Lead-Cooled Fast Reactors

Authors: Tan Jibo

Date: 2025-04-19T20:56:08+00:00

Abstract

The environmental compatibility of structural materials in liquid lead-bismuth is a bottleneck restricting the research, development, and construction of lead-cooled fast reactors. 9-12Cr ferritic/martensitic steels and austenitic stainless steels are preferred candidate materials for fuel cladding and reactor vessels, but they face severe liquid metal corrosion (oxidation and dissolution) in high-temperature liquid lead-bismuth environments; typically, appropriate amounts of Si or Al are added to alloys to improve their resistance to liquid lead-bismuth corrosion. This paper reviews research progress on corrosion, dissolution, slow strain rate tensile testing, creep, fatigue, and crack propagation of 9-12Cr ferritic/martensitic steels, austenitic stainless steels, Si-enhanced ferritic/martensitic and austenitic stainless steels, and Al-containing austenitic stainless steels in liquid lead-bismuth environments, discusses the liquid metal embrittlement susceptibility and damage mechanisms of ferritic/martensitic steels (body-centered cubic) and austenitic stainless steels (face-centered cubic) in liquid lead-bismuth environments, identifies existing problems in current research, and outlines future research directions.

Full Text

Preamble

Research Progress on Environmental Compatibility of Stainless Steels for Lead-Cooled Fast Reactors

Jibo Tan, Xinqiang Wu*

Key Laboratory of Nuclear Materials and Safety Assessment, Institute of Metal Research, Chinese Academy of Sciences, Shenyang 110016, China

Abstract

The environmental compatibility of structural materials in liquid lead-bismuth eutectic (LBE) represents a critical bottleneck for the development and deployment of lead-cooled fast reactors. 9-12Cr ferritic/martensitic steels and austenitic stainless steels are preferred candidate materials for fuel cladding and reactor vessels, yet they face severe liquid metal corrosion (oxidation and dissolution) in high-temperature LBE environments. Alloying with appropriate amounts of Si or Al is commonly employed to enhance corrosion resistance. This review synthesizes recent advances in understanding the corrosion, dissolution, slow strain rate tensile behavior, creep, fatigue, and crack propagation of 9-12Cr ferritic/martensitic steels, austenitic stainless steels, Si-enhanced variants, and Al-containing austenitic stainless steels in liquid LBE. We discuss the liquid metal embrittlement sensitivity and damage mechanisms of ferritic/martensitic steels (body-centered cubic) versus austenitic stainless steels (face-centered cubic) in LBE, identify current research gaps, and outline future research directions.

Keywords: Lead-cooled fast reactor; Stainless steel; Liquid metal corrosion; Liquid metal embrittlement; Mechanical properties

Author Information: Jibo Tan, male, born 1988, researcher

Corresponding Author: Xinqiang Wu, E-mail: xqwu@imr.ac.cn, researcher, specialist in nuclear materials environmental compatibility

Funding: National Natural Science Foundation of China (No. U23B2074), CNNC Science Fund for Talented Young Scholars (No. E241F103Z1), Liaoning Provincial Excellent Youth Foundation (No. 2024JH3/10200020), Chinese Academy of Sciences Strategic Priority Research Program (No. XDA0410403)

China is actively developing nuclear power in a safe and orderly manner, implementing the “three-step” strategy of thermal reactors → fast reactors → fusion reactors. While commercial pressurized water reactors currently dominate, advanced reactor types including lead-cooled fast reactors, sodium-cooled fast reactors, and thorium-based molten salt reactors are under active development. Lead-cooled fast reactors employ a closed fuel cycle, achieving uranium utilization exceeding 80% (compared to <1% for U-235 in PWR fuel), thereby supporting sustainable uranium resource utilization. Pure lead or lead-bismuth eutectic alloys offer advantages including low melting point, high boiling point, favorable neutron economy, and chemical inertness, making them preferred coolants for lead-cooled fast reactors [1-3]. Internationally, multiple lead-cooled fast reactor designs have been proposed, including Europe’s ELFR, Russia’s BREST-OD-300 and SVBR-100, America’s SSTAR, Korea’s URANUS-40, China’s CLEAR-I, and Japan’s PBWFR, with key parameters summarized in [3]. Lead-cooled fast reactors typically have design lifetimes of 15-30 years, operating temperatures of 300-650°C, liquid lead or LBE flow velocities up to 2 m/s, and fast neutron

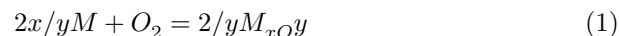
irradiation doses up to 150 dpa (displacements per atom). Critical components such as fuel cladding and reactor vessels experience coupled damage from irradiation, high temperature, complex stress states, and liquid LBE corrosion during service. Consequently, key materials must satisfy stringent requirements: (1) excellent resistance to irradiation swelling to maintain dimensional stability; (2) good resistance to irradiation hardening and embrittlement; (3) comprehensive mechanical properties including high-temperature strength, ductility, creep resistance, fatigue performance, and creep-fatigue behavior; and (4) superior environmental resistance in liquid LBE, including oxidation, dissolution, and liquid metal embrittlement resistance [2,4].

Due to their excellent high-temperature mechanical properties and irradiation damage resistance, combined with extensive service data from fossil power plants and irradiation damage data from fusion reactor first-wall applications [5], 9-12Cr ferritic/martensitic steels are preferred fuel cladding materials for lead-cooled fast reactors. Austenitic stainless steels, with their good strength, ductility, and corrosion resistance, plus extensive operational data from PWRs, are preferred reactor vessel materials. Novel materials such as FeCrAl alloys, high-entropy alloys, and SiC, which exhibit outstanding oxidation resistance, are also candidate materials for critical components [2]. This review summarizes research progress on the damage behavior of 9-12Cr ferritic/martensitic steels, austenitic stainless steels, and their modified variants (Si-enhanced ferritic/martensitic and austenitic steels, Al-containing austenitic stainless steels) in liquid LBE environments.

1. Corrosion Thermodynamic Analysis

Corrosion of high-Cr steels containing Al and Si, Fe-Al coatings, and SiC in liquid LBE primarily involves dissolution and oxidation. [Figure 1: see original paper] presents solubility curves for various metallic elements in liquid LBE, revealing that metallic elements exhibit relatively high solubility in high-temperature LBE, particularly Ni, Mn, and Cu [1]. Consequently, alloys with high Ni, Mn, or Cu content, such as nickel-based superalloys, are generally unsuitable for lead-cooled fast reactor core components. However, Ni, Mn, and Cu are typical austenite-stabilizing elements essential for single-phase face-centered cubic alloys like 316 stainless steel. To mitigate dissolution corrosion effectively, protective oxide films must form on the surface to prevent intimate contact between the substrate and liquid LBE.

The oxidation of alloying elements in liquid LBE, under standard atmospheric pressure, consumes 1 mol O_2 to form oxide $M O$ according to reaction (1):



where M represents an alloying element. Thermodynamic data [6] enable calculation of the Gibbs free energy change (ΔG° , kJ/mol) for $M O$ formation.

Oxide stability thermodynamically depends on temperature and oxygen partial pressure. The ΔG° , enthalpy change (ΔH° , kJ/mol), entropy change (ΔS° , J/mol·K), and temperature (T, K) relationships for common oxides in liquid LBE are listed in . The dissolved oxygen concentration in liquid LBE follows Sievert's law, with the relationship between oxygen partial pressure (p_{O_2} , bar) and dissolved oxygen concentration (C_{O} , wt.%) given by equation (2) [7]:

$$C_O = \exp\left(13.558 - \frac{12986}{T}\right) \cdot \sqrt{p_{O_2}} \quad (2)$$

The relationship between ΔG and p_{O_2} is expressed by equations (3) and (4) [7]:

$$\Delta G = \Delta G^\circ + RT \ln p_{O_2} \quad (3)$$

$$\Delta G = RT \ln p_{O_2} \quad (4)$$

where R is the gas constant (8.3145 J/mol·K). Based on these relationships, Gibbs free energy-temperature-dissolved oxygen concentration diagrams can be constructed to determine the thermodynamic stability of oxides under various temperature and dissolved oxygen conditions, as shown in [Figure 2: see original paper]. The oxygen affinity of elements in liquid LBE follows the sequence Al > Ti > Si > Cr > Fe > Ni > Pb, indicating that Al, Ti, Si, and Cr oxides exhibit high stability in high-temperature LBE. Since Ni shows extremely high solubility in liquid LBE and its oxides have poor stability, high-temperature nickel-based alloys are unsuitable for reactor core components. Al, Ti, and Si serve as corrosion-resistant elements, typically added to 9-12Cr ferritic/martensitic steels and austenitic stainless steels to improve liquid LBE corrosion resistance. Notably, oxidation in liquid LBE also depends on the activity of elements in the alloy, as expressed by equation (5) [8-10]:

$$\Delta G = \Delta G^\circ + RT \ln a_M \quad (5)$$

where a_M is the activity of element M in the alloy, typically <1. Consequently, the minimum dissolved oxygen concentration required for oxide formation in the alloy is usually higher than the predicted values in [Figure 2: see original paper].

[Figure 1: see original paper]

[Figure 2: see original paper]

2. 9-12Cr Ferritic/Martensitic Steels

2.1 Corrosion Behavior in Liquid LBE

9-12Cr ferritic/martensitic steels exhibit excellent resistance to neutron irradiation swelling and good high-temperature creep performance ($<600^{\circ}\text{C}$), making them preferred fuel cladding materials for lead-cooled fast reactors. Major grades include T91, P92, HT-9, E911, and Manet II [2,11-13], typically containing $0.5\text{ wt.}\% \text{O}_4$ and FeCr_2O_4 oxide films typically form on the surface, providing effective protection against severe oxidation and dissolution corrosion. At temperatures above 550°C , porous outer Fe_3O_4 layers, dense inner FeCr_2O_4 layers, and Cr-selective internal oxidation zones form under high-oxygen conditions, while dissolution corrosion occurs under low-oxygen conditions [13-20]. [Figure 3: see original paper] shows typical cross-sectional morphologies of oxide films on T91 steel after 1000 h exposure in LBE at 550°C under various oxygen concentrations: oxidation occurs at dissolved oxygen concentrations above $1.26 \times 10^{-6} \text{ wt.}\%$, while LBE penetration and dissolution corrosion dominate below $1.41 \times 10^{-8} \text{ wt.}\%$ [13]. Additionally, high LBE flow velocities ($\sim 2 \text{ m/s}$) can erode the oxide film on ferritic/martensitic steel surfaces, promoting direct contact between the substrate and liquid LBE and accelerating mass transfer, which further degrades oxidation and dissolution resistance [15,16,19].

To enhance the liquid LBE corrosion resistance of 9-12Cr ferritic/martensitic steels, 1-2 wt.% Si is typically added to promote formation of dense Si-rich oxide films that effectively protect the substrate. Typical Si-enhanced ferritic/martensitic steel grades and their chemical compositions are listed in . Wang et al. [21] reported that Si content must exceed 0.5 wt.% in 9Cr ferritic/martensitic steel to effectively improve liquid LBE corrosion resistance. M.P. Short et al. [22] investigated the corrosion behavior of Fe-2Cr-2Si in liquid LBE at $600\text{-}715^{\circ}\text{C}$ (506 h), finding that Fe-, Cr-, and Si-rich oxide films formed on the surface, particularly nanoscale Si-rich oxides in the inner layer, which significantly enhanced corrosion resistance in both high- and low-oxygen LBE environments. Rong et al. [23,24] reported that the oxidation rate of 12Cr-Si steel in dynamic oxygen-controlled LBE at 550°C (0.3 m/s , $10^{-7}\text{-}10^{-6} \text{ wt.}\%$, 10,000 h) was approximately half that of HT-9 steel, primarily due to Si- and Cr-rich oxides formed at the oxide/substrate interface. Pre-oxidation in 1% oxygen atmosphere at 720°C for 1 h further improved corrosion resistance in liquid LBE. Polekhina et al. [25] studied long-term corrosion of EP-823-sh steel in dynamic oxygen-controlled LBE at 630°C ($4\text{-}8 \times 10^{-7} \text{ wt.}\%$, $\sim 2 \text{ m/s}$, 2500 h), observing non-uniform oxide films ($0.25\text{-}18 \text{ }\mu\text{m}$) composed of Si- and Mn-containing Fe-Cr spinels, with $(\text{Si,Cr,Mn})_2\text{O}_3$ preferentially growing along grain boundaries in the internal oxidation zone. EP-823-sh steel, with its excellent mechanical and corrosion properties, has been selected as fuel cladding material for Russia's BREST-OD-300 lead-cooled fast reactor [26,27]. Russia has also developed high-Si (1.9 wt.%) EI-852 ferritic/martensitic steel, though it exhibits significant irradiation embrittlement [27]. Yang et al. [28] developed SIMP steel, demonstrating superior irradiation resistance, high-temperature oxidation resis-

tance, liquid LBE corrosion resistance, and creep performance (550°C) compared to T91 steel. Lu et al. [29] also developed 9Cr-Si ferritic/martensitic steel, finding that Si addition effectively improved corrosion resistance in static oxygen-saturated LBE at 550°C.

However, Schroer et al. [30] investigated 1.4718 ferritic/martensitic steel in dynamic oxygen-controlled LBE at 450°C and 550°C (10^{-7} - 10^{-6} wt.%, 2 m/s, 1200-15,000 h), finding significantly improved corrosion resistance compared to T91 at 450°C but minimal effect at 550°C. At 550°C, the oxide film exhibited a thin outer spinel layer and a deep Si-selective internal oxidation zone along grain boundaries. Shi et al. [31] similarly found that 9Cr ferritic/martensitic steels with 0.7-1 wt.% Si, after 2000 h exposure in oxygen-controlled LBE (10^{-6} wt.%) at 550°C and 600°C, developed thinner outer spinel oxide films and deeper Si-selective internal oxidation zones, suggesting that altered oxide film structure enhanced substrate/oxide adhesion and improved corrosion resistance, as shown in [Figure 4: see original paper]. In summary, Si addition (~1%) promotes formation of Si-rich oxide films and enhances liquid LBE corrosion resistance of 9-12Cr ferritic/martensitic steels, particularly for 12Cr grades.

[Figure 3: see original paper]

[Figure 4: see original paper]

The synergistic effects of irradiation and liquid LBE can significantly influence fuel cladding corrosion behavior. Yao et al. [32] studied in-situ Ar^+ irradiation (1.36 dpa) coupled with dynamic liquid LBE corrosion (350°C, saturated oxygen, 0.6 m/s, 92 h) of SIMP steel (11Cr, 1.43Si), finding that irradiation enhanced elemental diffusion and accelerated oxidation, increasing oxide film thickness from 110 nm (0 dpa) to 500 nm (1.36 dpa). Frazer et al. [33] investigated in-situ proton irradiation (~22 dpa) coupled with liquid LBE corrosion (420°C, saturated oxygen, 80 h) of HT-9 ferritic/martensitic steel (12Cr, 0.4Si), also observing irradiation-accelerated oxidation with oxide film thickness increasing from 1 μm to 13 μm . Demir et al. [34] recently studied Fe-12Cr-2Si alloy under in-situ proton irradiation-liquid LBE corrosion (4 h), finding that at 675°C in low-oxygen LBE, the alloy formed Cr- and Si-rich oxides that effectively protected the substrate from LBE attack, with minimal irradiation effect on corrosion behavior. However, current studies on structural material corrosion in simulated irradiation-LBE environments have experimental durations <100 h, whereas lead-cooled fast reactor design lifetimes typically reach 15-30 years, necessitating long-term irradiation-corrosion data for component life design and safety assessment.

2.2 Mechanical Behavior in Liquid LBE

The mechanical performance of ferritic/martensitic steels in liquid LBE critically affects component safety, encompassing slow strain rate tensile behavior, fatigue, creep, and crack propagation. Numerous studies have evaluated liquid metal embrittlement sensitivity of 9-12Cr ferritic/martensitic steels through

slow strain rate tensile tests, with key influencing factors including temperature, dissolved oxygen concentration, strain rate, irradiation hardening, and Si content [35-44]. Results show that elongation-temperature curves typically exhibit a “ductility trough,” with minimum plasticity and maximum embrittlement sensitivity around 350°C, characterized by quasi-cleavage fracture features [40,41] as shown in [Figure 5: see original paper]. At low dissolved oxygen concentrations, protective oxide films cannot form, allowing direct LBE-substrate contact, dissolution corrosion, and quasi-cleavage cracking, significantly reducing ductility. Strain rate affects embrittlement sensitivity by influencing oxide film rupture/repair and LBE-substrate contact time; higher strain rates increase embrittlement sensitivity under saturated oxygen conditions, while lower strain rates increase sensitivity under low-oxygen conditions. Irradiation effects correlate with hardening degree: when irradiation and test temperatures are comparable, irradiation hardening enhances embrittlement sensitivity; when irradiation temperature exceeds test temperature, no hardening occurs and sensitivity remains unchanged [42]. Although Si addition improves liquid LBE corrosion resistance, it promotes Laves phase precipitation, raising the ductile-to-brittle transition temperature [24]. First-principles calculations indicate that Si significantly reduces surface energy and Young’s modulus, increasing embrittlement sensitivity of BCC Fe in liquid LBE [44]. However, systematic studies on slow strain rate tensile behavior of Si-enhanced ferritic/martensitic steels in liquid LBE are lacking.

Factors affecting low-cycle fatigue performance of ferritic/martensitic steels in liquid LBE include strain amplitude, temperature, dissolved oxygen concentration, and strain rate [45-51]. T91 steel fatigue life in LBE increases with decreasing strain amplitude, with environmental effects more pronounced at high strain amplitudes [Figure 6a: see original paper] [45]. Fatigue life-temperature curves exhibit “valley and peak” characteristics: T91 steel fatigue life increases with temperature in 150-250°C and 350-500°C ranges, but decreases in 250-350°C and 500-550°C ranges [46,47]. T91 steel fatigue life in saturated-oxygen LBE typically exceeds that in oxygen-poor conditions [Figure 6a: see original paper], though studies at high temperature (550°C) are needed. Strain rate effects depend on temperature: at 350°C, strain rate has minimal impact on T91 steel fatigue life [Figure 6c: see original paper] [45], but at 550°C in saturated-oxygen LBE, fatigue life decreases significantly with decreasing strain rate (0.004-0.4% s⁻¹) [Figure 6d: see original paper] [48]. Current research on corrosion fatigue behavior of ferritic/martensitic steels focuses on low temperatures (≤ 350°C), requiring systematic investigation at typical service temperatures (550°C).

Fracture toughness, creep, and crack propagation properties of ferritic/martensitic steels are also significantly degraded in liquid LBE. Studies show that creep rates of T91, P92, and HT-9 steels in LBE at 550-650°C may increase by up to 50 times [11,12,37,52]. FeCrAl coatings on T91 steel can improve creep resistance in LBE at 550°C [53]. Fracture toughness of T91 steel in LBE at 200-355°C decreases compared to air, typically reducing with decreasing tensile rate by up to ~30% [54-58]. Fatigue crack propagation

rates of T91 steel in LBE at 150–450°C increase significantly compared to air (saturated oxygen, load ratio 0.1, frequency 0.1 Hz), with LBE wetting crack tips, diffusion/adsorption into the substrate, and quasi-cleavage cracking accelerating crack growth [59,60].

[Figure 5: see original paper]

[Figure 6: see original paper]

3. Austenitic Stainless Steels

3.1 Corrosion Behavior in Liquid LBE

Austenitic stainless steels, with their excellent fracture toughness, corrosion resistance, and intermediate-to-high temperature mechanical properties, are preferred reactor vessel materials for lead-cooled fast reactors, with major grades including 316, 304, and 15-15Ti [2,24,61–63]. Environmental compatibility studies reveal that in high-oxygen LBE, austenitic stainless steels develop porous outer Fe_3O_4 and dense inner FeCr_2O_4 oxide films [16,24,61–66]. Below 450°C, these films effectively protect the substrate, but above 450°C, they become ineffective, with severe intergranular oxidation occurring under high-oxygen conditions and dissolution corrosion under low-oxygen conditions. Ni preferential dissolution can cause ferritization of the substrate. [Figure 7: see original paper] shows typical cross-sectional morphology of oxide films on 316L stainless steel after 2000 h exposure in saturated-oxygen LBE at 550°C, exhibiting intergranular oxidation, particularly at high-angle grain boundaries [62]. High LBE flow velocity (~2 m/s) can erode the oxide film, promoting Ni dissolution and intensifying dissolution corrosion [66].

Si addition improves corrosion resistance by forming dense Si-rich oxide films. Typical chemical compositions of Si-enhanced austenitic stainless steels are listed in . Schroer et al. [67] studied long-term corrosion (40,000 h) of 1.4571 stainless steel (1 wt.% Si) in dynamic oxygen-controlled LBE at 550°C (2 m/s, 10^{-9} – 10^{-5} and 10^{-6} wt.%). Specimens exposed to low oxygen (10^{-9} – 10^{-5} wt.%) suffered severe dissolution corrosion, while those at 10^{-6} wt.% oxygen formed protective Cr-Si-rich oxide films in some regions, with dissolution in others. Kurata et al. [68] investigated 18Cr-20Ni-5Si steel in static LBE at 450°C and 550°C, finding that after 3000 h, a continuous submicron Si-rich oxide film formed, providing excellent corrosion resistance. Roy et al. [69] studied 18Cr-15Ni-3.7Si and 21Cr-11Ni-1.6Si steels in static LBE at 520°C (10^{-9} – 10^{-4} wt.% oxygen for first 30 h, then 10^{-4} wt.%), observing nanoscale oxide films with good corrosion resistance after 1850 h. Chen et al. [24,70–72] developed Fe-15Cr-9Ni-2Si stainless steel based on 316 steel; after 3000 h in static saturated-oxygen LBE at 550°C, the oxide film consisted of porous outer Fe_3O_4 and dense inner Fe-Cr spinel with uniformly distributed nanoscale SiO_2 particles in the spinel and at oxide/substrate interface voids [Figure 8: see original paper]. Unlike 316 steel, which suffers severe intergranular oxidation at 550°C, Fe-15Cr-9Ni-2Si steel showed no significant intergranular oxidation, likely due to enhanced

oxide film densification from SiO_2 particles hindering elemental diffusion. Wu et al. [24] also reported that Si-enhanced austenitic stainless steels exhibit significantly reduced oxidation rates compared to 316H in static saturated-oxygen LBE at 550°C , and no dissolution corrosion after 1500 h in dynamic oxygen-controlled LBE (0.3 m/s, 10^{-6} - 10^{-7} wt.%), attributed to Si enrichment in the inner oxide layer. However, Kurata et al. [73,74] reported that Si-enhanced austenitic stainless steels (2.4-5.8 wt.% Si) still experience dissolution corrosion during long-term exposure in low-oxygen (10^{-8} wt.%) LBE at 550°C . In summary, appropriate Si addition improves oxidation and dissolution resistance of austenitic stainless steels in LBE, representing a primary direction for reactor vessel material development.

Al addition also enhances corrosion resistance. Al-containing austenitic stainless steels typically have compositions of Fe-(12-35)Ni-(12-20)Cr-(2-6)Al-(0.1-3)Nb. Zhang et al. [75,76] studied Fe-23Ni-15Cr-3Al steel in LBE at 600°C , observing dissolution corrosion at 10^{-8} wt.% oxygen, formation of ~ 100 nm Cr-Al-rich oxide films with continuous Al_2O_3 at the oxide/substrate interface at 10^{-6} wt.% oxygen, and ~ 5 μm oxide films (outer Fe_3O_4 + minor Cr-Al-rich oxides, intermediate Fe-Cr spinel, inner Cr-rich oxide + minor Al-rich oxide) with localized dissolution in saturated oxygen. Cold-work-induced dislocations and grain boundaries promoted Cr and Al diffusion, facilitating rapid formation of protective oxide films. Shen et al. [77] investigated Fe-14Ni-14Cr-2.5Al steel in dynamic oxygen-controlled LBE at 550°C (1.8 m/s, 5×10^{-7} - 5×10^{-6} wt.%), finding continuous nanoscale Al-rich oxide films with excellent corrosion resistance. Tsisar et al. [78] studied long-term corrosion (10,000 h) of Fe-14Cr-2Mn-20Ni-0.5Cu-3Al and Fe-14Cr-5Mn-12Ni-3Cu-2.5Al steels in static LBE at 500°C (10^{-9} - 10^{-6} wt.% oxygen), observing submicron Al-Cr-rich oxide films with good corrosion resistance, though high-Ni steel experienced localized dissolution corrosion under low oxygen (10^{-9} wt.%). These results demonstrate that Al-containing austenitic stainless steels form Al-rich oxide films, particularly continuous Al_2O_3 at the oxide/substrate interface, providing excellent corrosion resistance, though localized dissolution corrosion remains a risk under low-oxygen conditions ($<10^{-8}$ wt.%).

[Figure 7: see original paper]

[Figure 8: see original paper]

[Figure 9: see original paper]

3.2 Mechanical Behavior in Liquid LBE

Research on austenitic stainless steel mechanical behavior in liquid LBE has focused on slow strain rate tensile, creep, fatigue, and crack propagation properties. Sapundjiev et al. [79] conducted slow strain rate tensile tests (5×10^{-6} s $^{-1}$) on 316L stainless steel in LBE at 200°C , finding no embrittlement in either unirradiated or irradiated (1.5 dpa) conditions. Bosch et al. [80] and Stergar et al. [81] similarly reported no embrittlement of irradiated 316L steel (1.5 dpa)

in LBE at 200, 350, and 450°C. Petersson et al. [82] performed slow strain rate tests (140–600°C, 5×10^{-5} s⁻¹) on Al-containing austenitic stainless steels in low-oxygen LBE (10⁻¹⁰ wt.%), observing no embrittlement below 550°C but intergranular cracking above 570°C. Serre et al. [83] also reported reduced elongation and liquid metal embrittlement of Al-containing austenitic stainless steels in liquid lead above 500°C. Gong et al. [84] studied creep behavior of 15-15Ti steel in LBE at 550°C and 600°C (10⁻¹⁰ wt.%-saturated oxygen), finding significantly increased creep rates due to dissolution corrosion and intergranular cracking.

Yas'kiv et al. [85] investigated low-cycle fatigue of Fe-18Cr-10Ni in liquid lead at 350°C, showing fatigue life decreased significantly with increasing strain amplitude. Ding et al. [86] studied low-cycle fatigue of 316LN stainless steel tubular specimens (filled internally with LBE) at 400°C, finding fatigue life decreased only at high strain amplitudes ($0.8 \times 400^\circ\text{C}$), requiring systematic investigation at typical service temperatures (400–500°C).

[Figure 10: see original paper]

4. Liquid Metal Embrittlement Mechanism

Liquid metal embrittlement causes severe degradation of structural material properties including ductility, fracture toughness, creep, and fatigue, posing a major threat to safe operation of lead-cooled fast reactors. Body-centered cubic metals exhibit high embrittlement sensitivity, while face-centered cubic metals show lower sensitivity. The primary characteristics of embrittlement in liquid LBE include reduced plasticity and quasi-cleavage fracture features. [Figure 11: see original paper] shows typical quasi-cleavage fracture morphologies on T91 steel after low-cycle fatigue (bar specimens) and fatigue crack propagation (CT specimens) tests in saturated-oxygen LBE at 350°C [46,59].

Various models have been proposed for liquid metal embrittlement in solid/liquid metal systems, including adsorption-induced surface energy reduction, adsorption-induced atomic bond weakening, adsorption-promoted dislocation emission, adsorption-enhanced work hardening, and stress-assisted dissolution [2]. T91 steel exhibits severe embrittlement in specific LBE environments, with macroscopic transgranular quasi-cleavage and microscopic cracking along deformation-induced grain boundaries and high-density dislocation interfaces. No single model fully explains T91 steel embrittlement. Gong et al. [45,51] proposed a mechanism based on adsorption-induced atomic bond weakening: LBE adsorption weakens atomic bonds at crack tips while dislocation pile-up causes material hardening; when the critical stress for dislocation motion exceeds the weakened bond strength, atomic bond rupture leads to cleavage fracture. Xue et al. proposed that fatigue brittle cracks in T91 steel at 150–450°C in LBE appear transgranular macroscopically but propagate along 1–5° subgrain boundaries formed by local plastic deformation at crack tips. Atomic-scale characterization [Figure 12: see original paper]

revealed that LBE wets the plastic deformation zone at crack tips, with Pb-Bi atom segregation, short-range ordered Pb/Bi-Fe superstructures, and Pb-Bi clusters/precipitates/films observed on deformation subgrain boundaries. Intergranular Pb-Bi atoms reduce atomic bonding strength, forming microcracks along subgrain boundaries and initiating brittle fracture. These atomic-scale results elucidate the quasi-cleavage embrittlement mechanism of T91 steel. Additionally, at 550°C in saturated-oxygen LBE, fatigue crack tips in T91 steel undergo dynamic recrystallization with severe grain boundary oxidation and Pb-Bi penetration, reducing grain boundary cohesion and causing oxidation+Pb-Bi penetration-dominated embrittlement [48].

Although slow strain rate tensile and low-cycle fatigue tests of 316L(N) stainless steel in LBE show ductile fracture features with low embrittlement sensitivity, Xue et al. reported that fatigue crack propagation rates of 316LN steel in saturated-oxygen LBE at 300°C and 400°C exceeded those in air, with quasi-cleavage features on fracture surfaces indicating liquid metal embrittlement. [Figure 13: see original paper] shows microstructural features at fatigue crack tips in 316LN steel at 400°C in saturated-oxygen LBE: Pb-Bi atoms preferentially diffuse along deformation twin boundaries and dislocation interfaces with concurrent Ni selective dissolution, forming Pb_7Bi_3 particles, Pb-Bi segregation, microvoids, and interface cracking that reduce cohesion and promote brittle crack propagation along microstructural interfaces. Serre et al. [83] also observed reduced elongation and intergranular cracking in Al-containing austenitic stainless steels in high-temperature liquid lead (500°C), indicating liquid metal embrittlement. Luo et al. [91] observed Bi atoms forming bilayer or trilayer structures at Ni grain boundaries, where liquid Bi splits the boundary into two grains each covered by Bi monolayers, with Bi-Bi bond strength much lower than Ni-Ni bonds, causing Ni embrittlement. Yu et al. [92] observed segregation-induced ordered superstructures at general grain boundaries in Ni-Bi systems that cause polycrystalline alloy embrittlement. Duscher et al. [93] studied Cu/Bi systems, finding that grain boundary segregation of Bi atoms embrittles copper by inducing Zn-like electronic structures in surrounding Cu atoms. Thus, despite lower embrittlement sensitivity of face-centered cubic alloys, Pb-Bi penetration and segregation along grain boundaries, deformation twin boundaries, and high-density dislocation interfaces can still cause quasi-cleavage cracking.

[Figure 11: see original paper]

[Figure 12: see original paper]

[Figure 13: see original paper]

5. Summary and Outlook

- (1) 9-12Cr ferritic/martensitic steels and 316 stainless steel are preferred fuel cladding and reactor vessel materials for lead-cooled fast reactors. However, Fe_3O_4 and $FeCr_2O_4$ oxide films formed at high temperatures

(>450°C) in liquid LBE cannot effectively protect the substrate, leading to severe oxidation corrosion with intergranular oxidation under high-oxygen conditions and dissolution corrosion under low-oxygen conditions, with corrosion resistance further deteriorating at high flow velocities (~2 m/s).

- (2) Adding appropriate Si or Al to 9-12Cr ferritic/martensitic and austenitic stainless steels promotes formation of Si-rich oxide films that effectively improve liquid LBE corrosion resistance. Current developments include Si-enhanced ferritic/martensitic steels (1-2 wt.% Si), Si-enhanced austenitic stainless steels (2.5-5 wt.% Si), and Al-containing austenitic stainless steels (2-6 wt.% Al). However, dissolution corrosion risks remain in high-temperature, low-oxygen (10^{-8} wt.%) LBE.
- (3) 9-12Cr ferritic/martensitic steels exhibit high liquid metal embrittlement sensitivity in LBE, typically undergoing quasi-cleavage cracking (~450°C) or intergranular cracking (~550°C) under load, degrading ductility, fracture toughness, fatigue, creep, and crack propagation properties. The quasi-cleavage embrittlement mechanism involves LBE wetting of the plastic deformation zone at crack tips, forming Pb-Bi segregation, short-range ordered Pb/Bi-Fe superstructures, and Pb-Bi clusters/precipitates/films on deformation subgrain boundaries that reduce atomic bonding strength. High-temperature intergranular cracking results from combined grain boundary oxidation and LBE penetration.
- (4) 316L(N) stainless steel shows low liquid metal embrittlement sensitivity in LBE, typically exhibiting ductile fracture with ductility, fracture toughness, and fatigue performance comparable to or slightly lower than in air. However, quasi-cleavage cracking occurs during fatigue crack propagation due to Pb-Bi penetration and segregation along grain boundaries, deformation twin boundaries, and high-density dislocation interfaces.
- (5) Limited research exists on creep, fatigue, and creep-fatigue behavior of ferritic/martensitic and austenitic stainless steels at typical service temperatures (500-550°C) in liquid LBE. Intergranular oxidation occurs at high temperatures, and corrosion-stress interaction may degrade service performance, requiring systematic investigation.
- (6) Si and Al are ferrite-stabilizing elements that typically reduce fracture toughness, increase ductile-to-brittle transition temperature, and worsen irradiation embrittlement resistance when added to ferritic/martensitic and austenitic stainless steels. Current research has primarily focused on corrosion behavior of Si-enhanced ferritic/martensitic steels, Si-enhanced austenitic stainless steels, and Al-containing austenitic stainless steels in liquid LBE. Systematic studies of their service behavior and damage mechanisms under simulated irradiation-thermal-mechanical-corrosion coupling conditions are needed to support engineering applications in lead-cooled fast reactors.

[1] Handbook on Lead-Bismuth Eutectic Alloy and Lead Properties, Materials

- Compatibility, Thermal-hydraulics and Technologies [B], 2015, OECD/NEA No.6195.
- [2] X. Gong, M. P. Short, T. Auger, E. Charalampopoulou, K Lambrinou. Environmental degradation of structural materials in liquid lead-and lead-bismuth eutectic-cooled reactors [J]. *Prog. Mater. Sci.* 126 (2022) 100920.
- [3] Handbook of Generation IV Nuclear Reactors [B]. Chapter 6, Lead-cooled fast reactor, 2016, P119-155
- [4] G.S. Was. Challenges to the use of ion irradiation for emulating reactor irradiation[J]. *J. Mater. Res.* 30(2015) 1158-1182.
- [5] Huang Qunying, Li Chunjing, Li Yanfen, Liu Shaojun, Wu Yican, Li Jiangang, Wan Farong, Ju Xin, Shan Yiyin, Yu Jinnan, Zhu Shengyun, Zhang Pinyuan, Yang Jianfeng, Han Fusheng, Kong Mingguang, Li Heqin, Muroga Takeshi, Nagasaka Takuya. Research Progress on China Low Activation Martensitic Steel CLAM[J]. *Nuclear Science and Engineering*, 1(2007)41-49
- [6] W. M. Haynes. CRC Handbook of Chemistry and Physics [M]. Florida, 2016.
- [7] C.F.E. Schroer, J. Konys. Physical Chemistry of Corrosion and Oxygen Control in Liquid Lead and Lead-Bismuth Eutectic, in, 2007.
- [8] C.H. Xu, W. Gao, Y.D. He. High temperature oxidation behaviour of FeAl intermetallics-oxide scales formed in ambient atmosphere[J]. *Scr. Mater.* 42 (2000) 975-980.
- [9] J. Eldridge, K.L. Komarek. Thermodynamic properties of solid iron-aluminum alloys[J]. *Trans. Metall. Soc. AIME* 230 (1964) 226.
- [10] W. Wang, Z.G. Zhu, L.J. Yang, J.T. Lu, J.Y. Huang, J.B. Tan, W.J. Kuang. Superior corrosion resistance of a slurry FeAl coating on 316LN stainless steel in 550 °C liquid lead-bismuth eutectic[J]. *Corros. Sci.*, 227(2024) 111757
- [11] M. Yurechko, C. Schroer, A. Skrypnik. Creep-to-rupture of the steel P92 at 650° C in oxygen-controlled stagnant lead in comparison to air[J]. *J. Nucl. Mater.*, 432(1-3) (2013)
- [12] J. Xiao, Z. Zhong, T. Wen, X. Yu, H. Wang, K. Zhao, C. Liu, H. Zhuo, S.Qiu, G. Liu, Y. Li, X. Gong. Synergy of stress and corrosion in a 12Cr ferritic/martensitic steel exposed to static liquid lead-bismuth eutectic at 550 °C[J]. *Corros. Sci.* 222 (2023) 111404
- [13] Z. G. Zhu, Q. Zhang, J.B.Tan, X.Q.Wu, H.B. Ma, Z.Y. Zhang, Q.S. Ren, E.-H. Han, X. Wang. Corrosion behavior of T91 steel in liquid lead-bismuth eutectic at 550 °C: Effects of exposure time and dissolved oxygen concentration[J]. *Corros. Sci.* 204 (2022) 110405.
- [14] D. Sapundjiev, S. Van Dyck, W. Bogaerts. Liquid metal corrosion of T91 and A316L materials in Pb-Bi eutectic at temperatures 400-600oC[J]. *Corros. Sci.* 48 (2006): 577-94.
- [15] C. Schroer, Z. Voß, O. Wedemeyer, J. Novotny, J. Konys. Oxidation of steel T91 in flowing lead-bismuth eutectic (LBE) at 550°C[J]. *J. Nucl. Mater.*, 356 (2006) 189-197.
- [16] S.J. Tian. Growth and exfoliation behaviour of the oxide scale on 316L and T91 in flowing liquid lead-bismuth eutectic at 480oC[J]. *Oxid. Met.*

93(2020):183-194.

- [17] L. Luo, Z. Xiao, M. Zhang, Z. Jiang, J. Liu, W. Huang, L. Sun. Honeycomb structure with oxygen-poor pores at the top of magnetite layer on a martensitic steel CLAM exposed to lead-bismuth eutectic at 500 °C[J]. *Corros. Sci.* 204 (2022) 110410
- [18] V. Tsisar, S. Gavrilov, C. Schroer, E. Stergar. Long-term corrosion performance of T91 ferritic/martensitic steel at 400 °C in flowing Pb-Bi eutectic with 2–7 mass% dissolved oxygen[J]. *Corros Sci* 2020;174:108852.
- [19] V. Tsisar, C. Schroer, O. Wedemeyer, A. Skrypnik, J. Konys. Corrosion interaction of 9% Cr ferritic/martensitic steels at 450 and 550 °C with flowing Pb-Bi eutectic containing 10–7 mass% dissolved oxygen[J]. *J Nucl Eng Radiat Sci* 5 (2019)031201.
- [20] C. Schroer, V. Tsisar, A. Durand, O. Wedemeyer, A. Skrypnik, J. Konys. Corrosion in iron and steel t91 caused by flowing lead-bismuth eutectic at 400 °C and 10–7 mass% dissolved oxygen[J]. *J Nucl Eng Radiat Sci* (2019) 011006.
- [21] J. Wang, S.P. Lu, L.J. Rong, D.Z. L, Y.Y. Li. Effect of silicon on the oxidation resistance of 9 wt.% Cr heat resistance steels in 550 °C lead-bismuth eutectic[J]. *Corros. Sci.* 111 (2016)
- [22] M.P. Short, R.G. Ballinger, H.E. Hanninen. Corrosion resistance of alloys F91 and Fe-12Cr-2Si in lead-bismuth eutectic up to 715 °C[J]. *J. Nucl. Mater.* 434 (2013) 259-281.
- [23] Pan Xia, Zhang Yangpeng, Dong Zhihong, Chen Shenghu, Jiang Haichang, Rong Lijian. Effect of Pre-oxidation Treatment on Pb-Bi Corrosion Resistance of 12Cr Ferritic/Martensitic Steel[J]. *Acta Metallurgica Sinica*, 2024, 60(5): 639-649.
- [24] Wu Xinqiang, Rong Lijian, Tan Jibo, Chen Shenghu, Hu Xiaofeng, Zhang Yangpeng, Zhang Ziyu. Research Progress on Si-Enhanced Ferritic/Martensitic and Austenitic Stainless Steels with Pb-Bi Corrosion Resistance[J]. *Acta Metallurgica Sinica*, 2023, 59(4): 502-512.
- [25] N.A. Polekhina, I.Yu. Litovchenko, K.V. Almaeva, S.A. Akkuzin, V.V. Linnik, E.N. Moskvichev, V.M. Chernov, I.A. Naumenko, M.S. Saifutdinova, M.V. Leontieva-Smirnova. Special features of the surface layer structure of ferritic-martensitic EP-823-Sh steel after prolonged exposure to the flowing lead at 630 °C under low oxygen concentration[J]. *J. Nucl. Mater.* 572 (2022) 154039
- [26] R. Isayev, N. Pukhareva, E. Malinovskiy, E. Korenevski, P. Dzhumaeva. Corrosion of EP823 Steel Cladding Under Heavy Liquid-Metal-Coolant Reactor Conditions: A Review[J]. *Nucl. Sci. Eng.*, (2024)1-19
- [27] A.M. Dvoriashin, S.I. Porollo, Yu.V. Konobeev, N.I. Budylnkin, E.G. Mironova, A.G. Ioltukhovskiy, M.V. Leontyeva-Smirnova, F.A. Garner. Mechanical properties microstructure of three Russian ferritic/martensitic steels irradiated in BN-350 reactor to 50 dpa at 490°C[J]. *J. Nucl. Mater.* 367-370 (2007) 92-96
- [28] Yang Ke, Yan Wei, Wang Zhiguang, Shan Yiyin, Shi Quanqiang, Shi Xianbo, Wang Wei. Research Progress on SIMP Steel: A Novel High-Temperature, Irradiation-Resistant, and Liquid Metal Corrosion-Resistant

- Structural Material for Nuclear Applications[J]. *Acta Metallurgica Sinica*, 2016, 52(10): 1207-1221.
- [29] Lu Yanhong, Song Yuanyuan, Chen Shenghu, Rong Lijian. Effect of Al and Si on Mechanical Properties and Pb-Bi Corrosion Resistance of 9Cr2WVTa Steel[J]. *Acta Metallurgica Sinica*, 2016, 52(3): 298-306.
- [30] C. Schroer, V. Koch, O. Wedemeyer, A. Skrypnik, J. Konys. Silicon-containing ferritic/martensitic steel after exposure to oxygen-containing flowing lead-bismuth eutectic at 450 and 550°C[J]. *J. Nucl. Mater.* 469 (2016) 162-176.
- [31] H. Shi, H. Wang, R. Fetzer, A. Heinzl, A. Weisenburger, K. Wang, A. Jianu, G. Müller. Influence of Si addition on the corrosion behavior of 9 wt% Cr ferritic/ martensitic steels exposed to oxygen-controlled molten Pb-Bi eutectic at 550 and 600 °C[J]. *Corros. Sci.* 193 (2021) 109871.
- [32] C. Yao, H. Zhang, H. Chang. Structure of surface oxides on martensitic steel under simultaneous ion irradiation and molten LBE corrosion[J]. *Corros. Sci.*, 195, (2022) 109953
- [33] S. Frazer, S. Qvist, Parker. Degradation of HT9 under simultaneous ion beam irradiation and liquid metal corrosion[J]. *J. Nucl. Mater.*, 479(2016) 382
- [34] E. Demir, S. Ayyapan, W. Zhou, W. Cairang, K. B. Woller, M. P. Short, D. Kaoumi. Behavior of Fe-based alloys in a liquid lead-bismuth environment under simultaneous proton irradiation and corrosion[J]. *Acta Mater.* 284 (2025) 120578
- [35] D.G. Kolman. A review of recent advances in the understanding of liquid metal embrittlement[J]. *Corrosion* 75 (2019) 42-57.
- [36] X. Gong, E. Stergar, P. Marmy, S. Gavrilov. Tensile fracture behavior of notched 9Cr-1Mo ferritic-martensitic steel specimens in contact with liquid lead-bismuth eutectic at 350 °C[J]. *Mater. Sci. Eng. A* 692 (2017) 139-145.
- [37] H. Wang, X. Gong, J. Xiao, L. Chai, Z. Yu, H. Chen, K. Zhao, J. Zhou, G. Liu, Y. Chen, S. Qiu. Liquid metal embrittlement of 12Cr ferritic/martensitic steel thin-walled tubes exposed to liquid lead-bismuth eutectic[J]. *Corros. Sci.* 195 (2022) 110024.
- [38] Y. Dai, B. Long, X. Jia, H. Glasbrenner, K. Samec, F. Groeschel. Tensile tests and TEM investigations on LiSoR-2 to -4[J]. *J. Nucl. Mater.* 356 (2006) 256-263.
- [39] F. Di Gabriele, A. Doubková, A. Hojná. Investigation of the sensitivity to EAC of steel T91 in contact with liquid LBE[J]. *J. Nucl. Mater.* 376 (2008) 307-311.
- [40] B. Long, Z. Tong, F. Gröschel, Y. Dai. Liquid Pb-Bi embrittlement effects on the T91 steel after different heat treatments[J]. *J. Nucl. Mater.* 377 (2008) 219-224.
- [41] J. Liu, W. Yan, W. Sha, W. Wang, Y. Shan, K. Yang. Effects of temperature and strain rate on the tensile behaviors of SIMP steel in static lead bismuth eutectic[J]. *J. Nucl. Mater.* 473 (2016) 189-196.
- [42] B. Long, Y. Dai, N. Baluc. Investigation of liquid LBE embrittlement effects on irradiated ferritic/martensitic steels by slow-strain-rate tensile tests[J]. *J. Nucl. Mater.* 431 (2012) 85-90.
- [43] Z. Hamouche-Hadjem, T. Auger, I. Guillot, D. Gorse. Susceptibility to

LME of 316L and T91 steels by LBE: Effect of strain rate[J]. *J. Nucl. Mater.* 376 (2008) 317-321.

[44] X. Gong, L. Sun, F.F. Zhang, Y. Yin, X. Huang, H. Gong, Y. Liu. Effect of alloying elements on liquid metal embrittlement of pure BCC Fe in contact with liquid lead-bismuth eutectic: Experiments and first principles calculation[J]. *Corros. Sci.* 208 (2022) 110522.

[45] X. Gong, P. Marmy, B. Verlinden, M. Wevers, M. Seefeldt. Low cycle fatigue behavior of a modified 9Cr-1Mo ferritic-martensitic steel in lead-bismuth eutectic at 350 °C -Effects of oxygen concentration in the liquid metal and strain rate[J]. *Corros. Sci.* 94 (2015) 377-391.

[46] B. Xue, W. Wang, J. Tan, W. Kuang, X. Wu, Z. Zhang, X. Wang, W. Ke. Insights into the fatigue damage mechanism of T91 steel in liquid lead-bismuth eutectic at 150-550 °C[J]. *Corros. Sci.* 232 (2024) 112007.

[47] B. Xue, J. Tan, Z. Zhang, X. Wang, X. Wu, E.-H. Han, W. Ke. Effect of temperature on low in liquid lead-bismuth eutectic environment at cycle fatigue behavior of T91 steel 150-550 °C[J]. *Int. J. Fatigue* 167 (2023) 107344.

[48] B. Xue, J. Tan, X. Wu, Z. Zhang, X. Wang, W. Ke. Strain-rate dependent fatigue behavior of T91 steel at 550 °C of liquid lead-bismuth eutectic[J]. *Corros. Sci.* 240 (2024) 112433.

[49] X. Gong, P. Marmy, L. Qin, B. Verlinden, M. Wevers, M. Seefeldt. Temperature dependence of liquid metal embrittlement susceptibility of a modified 9Cr-1Mo steel under low cycle fatigue in lead-bismuth eutectic at 160-450 °C[J]. *J. Nucl. Mater.* 468 (2016) 289-298.

[50] X. Gong, P. Marmy, Y. Yin. The role of oxide films in preventing liquid metal embrittlement of T91 steel exposed to liquid lead-bismuth eutectic[J]. *J. Nucl. Mater.* 509 (2018) 401-407.

[51] X. Gong, P. Marmy, A. Volodin, B. Amin-Ahmadi, L. Qin, D. Schryvers, S. Gavrilov, E. Stergar, B. Verlinden, M. Wevers, M. Seefeldt. Multiscale investigation of quasi-brittle fracture characteristics in a 9Cr-1Mo ferritic-martensitic steel embrittled by liquid lead-bismuth under low cycle fatigue[J]. *Corros. Sci.* 102 (2016) 137-152.

[52] A. Jianu, G. Müller, A. Weisenburger, A. Heinzl, C. Fazio, V.G. Markov, A.D. Kashtanov. Creep-to-rupture tests of T91 steel in flowing Pb-Bi eutectic melt at 550°C[J]. *J. Nucl. Mater.* 394 (2009) 102-108.

[53] A. Weisenburger, A. Jianu, W. An, R. Fetzer, M.D. Giacco, A. Heinzl, G. Müller, V.G. Markov, A.D. Kashtanov. Creep, creep-rupture tests of Al-surface-alloyed T91 steel in liquid lead bismuth at 500 and 550°C[J]. *J. Nucl. Mater.* 431 (2012) 77-84.

[54] J. Van den Bosch, G. Coen, A. Almazouzi, J. Degrieck. Fracture toughness assessment of in liquid lead-bismuth eutectic[J]. *J. Nucl. Mater.* 385 (2009) ferritic-martensitic steel

[55] T. Auger, D. Gorse, Z. Hamouche-Hadjem, J. Van den Bosch, G. Coen, A. Almazouzi, A. Hojna, K. Dalikova, F. Di Gabriele, M. Serrano, A. Gessi, P. Agostini, J.B. Vogt, I. Serre. Fracture mechanics behavior of the T91 martensitic steel in contact with liquid lead-bismuth eutectic for application in an accelerator driven system[J]. *J. Nucl. Mater.* 415 (2011)

- [56] M.L. Martin, T. Auger, D.D. Johnson, I.M. Robertson. Liquid-metal-induced fracture mode of martensitic T91 steels[J]. *J. Nucl. Mater.* 426 (2012) 71-77.
- [57] B. Long, Y. Dai. Investigation of LBE embrittlement effects on the fracture properties of T91[J]. *J. Nucl. Mater.* 376 (2008) 341-345.
- [58] G. Coen, J. Van den Bosch, A. Almazouzi, J. Degrieck. Investigation of the effect of lead-bismuth eutectic on the fracture properties of T91 and 316L[J]. *J. Nucl. Mater.* 398 (2010) 122-128.
- [59] B. Xue, J. Tan, X. Wu, Z. Zhang, W. Kuang, Q. Jin, X. Wang, E.-H. Han, W. Ke. Insights into in liquid lead-bismuth eutectic at fatigue crack propagation mechanism of T91 steel 150-450 °C[J]. *Corros. Sci.* 236 (2024) 112264.
- [60] B. Xue, J. Tan, X. Wu, Z. Zhang, X. Wang. A novel monitoring system for fatigue crack length of compact tensile specimen in liquid lead-bismuth eutectic[J]. *Nucl. Eng. Technol.* 56 (2023) 1887-1894.
- [61] C. Li, Y. Liu, F. Zhang. Erosion-corrosion of 304N austenitic steels in liquid PbBi flow perpendicular to steel surface[J]. *Mat. Charact.*, 175 (2021) 111054
- [62] C. Lu, M. Wang, J. Tan, X. Hao, T. Liang, Y. Ma. The initial enrichment behavior of nickel during the oxidation of 15-15Ti at 550 °C in liquid lead-bismuth eutectic A new Ni-rich structure at grain boundary[J]. *Corros. Sci.* 244 (2025) 112664
- [63] S. Guo, J. Chen, Z. Ma, Q. Du, C. Lu, S. Xie, B. Long, D. Yun, L. Gu. The roles of Ni segregation on the oxidation kinetics of austenitic stainless steel 316L exposed to oxygen-containing liquid lead-bismuth eutectic (LBE) [J]. *Corros. Sci.* 244 (2025) 112644
- [64] O. Klok, K. Lambrinou, S. Gavrilov, E. Stergar, J. Lim, T. Van der Donck. Effect of deformation twinning on dissolution corrosion of 316L stainless steels in contact with static liquid lead-bismuth eutectic (LBE) at 500oC[J]. *J. Nucl. Mater.* 510 (2018):556-567.
- [65] Y. Kurata, M. Futakawa, S. Saito. Comparison of the corrosion behaviour of austenitic and ferritic/martensitic steels exposed to static liquid Pb-Bi at 450 and 550oC[J]. *J. Nucl. Mater.* 343(2005):333-340.
- [66] V. Tsisar, C. Schroer, O. Wedemeyer, A. Skrypnik, J. Konys. Effect of structural state and surface finishing on corrosion behaviour of 1.4970 austenitic steel at 400 and 500oC in flowing Pb-Bi eutectic with dissolved oxygen[J]. *J. Nucl. Eng. Rad. Sci.* 4 (2018) 041001.
- [67] Carsten Schroer, Olaf Wedemeyer, Josef Novotny, Aleksandr Skrypnik, Jürgen Konys. Long-term service of austenitic steel 1.4571 as a container material for flowing lead-bismuth eutectic[J]. *J. Nucl. Mater.* 418 (2011) 8-15
- [68] Y. Kurata, M. Futakawa. Excellent corrosion resistance of 18Cr-20Ni-5Si steel in liquid Pb-Bi[J]. *J. Nucl. Mater.* 325 (2004) 217-222
- [69] Marion Roy, Laure Martinelli, Kevin Ginestar, Jerome Favergeon, Gerard Moulin. Dissolution and oxidation behaviour of various austenitic steels and Ni rich alloys in lead-bismuth eutectic at 520 °C[J]. *J. Nucl. Mater.* 468 (2016) 153-163

- [70] A. Xie, S. Chen, L. Yin, N. He, C. Chen, L. Rong. Microstructural evolution of the inner oxide layer of a Si-modified austenitic stainless steel exposed to oxygen-saturated lead-bismuth eutectic (LBE): Toward the origin of LBE penetration[J]. *Corros. Sci.* 237 (2024) 112350
- [71] Wu Yang, Xie Ang, Chen Shenghu, Jiang Haichang, Rong Lijian. Corrosion Behavior of NbC in Nb-Containing Austenitic Stainless Steel in Liquid Pb-Bi Eutectic and Its Effect on Oxide Layer Formation[J]. *Acta Metallurgica Sinica*, 61(2) (2025) 287-296.
- [72] A. Xie, S. Chen, S. Chen, H. Jiang, L. Rong. Austenite decomposition behavior adjacent to δ -ferrite in a Si-modified Fe-Cr-Ni austenitic stainless steel during thermal aging at 550 oC[J]. *Acta Mater.* 272 (2024) 119948
- [73] Y. Kurata. Results of corrosion tests in liquid Pb-Bi at JAEA-temperature and oxygen concentration dependence, and corrosion properties of Si-enriched steels, in: OECD/NEA,
- [74] Y. Kurata. Corrosion behavior of Si-enriched steels for nuclear applications in liquid lead-bismuth[J]. *J. Nucl. Mater.* 437 (2013) 401-408
- [75] D. Zhang, X. Zhang, Y. Guo, J. Zhang, H. Ren, X. Zeng, Q. Yan. High-resolution characterization revealing the effect of dissolved oxygen in lead-bismuth eutectic (LBE) on oxide scale and subsurface phase transformation layer in alumina-forming austenitic (AFA) steel[J]. *Corros. Sci.* 245 (2025) 112671
- [76] D. Zhang, X. Zhang, X. Zeng, J. Zhang, H. Ren, F. Meng, Q. Yan. High-resolution characterization of cold working effects on the oxidation behavior of alumina-forming austenitic (AFA) steel in lead-bismuth eutectic (LBE) with 10-6 wt.% oxygen at 600 °C[J]. *Journal of Nuclear Materials* 607 (2025) 155691
- [77] L. Shen, G. Cao, D. Lang, H. Peng, Y. Wen. Fe-14Ni-14Cr-2.5Al steel showing excellent corrosion-resistance in flowing LBE at 550 °C and high temperature strength[J]. *J. Nucl. Mater.* 587 (2023) 154703
- [78] V. Tsisar, E. Stergar, S. Gavrilov, W. V. Renterghem, P. Louette, S. Lucas. Effect of variation in oxygen concentration in static Pb-Bi eutectic on long-term corrosion performance of Al-alloyed austenitic steels at 500 °C[J]. *Corros. Sci.* 195 (2022) 109963
- [79] D. Sapundjiev, A. Al Mazouzi, S. Van Dyck. A study of the neutron irradiation effects on the susceptibility to embrittlement of A316L and T91 steels in lead-bismuth eutectic, *J. Nucl. Mater.*[J]. 356 (2006) 229-236.
- [80] J. Van den Bosch, G. Coen, R.W. Bosch, A. Almazouzi. TWIN ASTIR: First tensile results of T91 and 316L steel after neutron irradiation in contact with liquid lead-bismuth eutectic[J]. *J. Nucl. Mater.* 398 (2010) 68-72.
- [81] E. Stergar, S.G. Eremin, S. Gavrilov, M. Lambrecht, O. Makarov, V. Iakovlev. Influence of LBE long term exposure and simultaneous fast neutron irradiation on the mechanical properties of T91 and 316L[J]. *J. Nucl. Mater.* 473 (2016) 28-34.
- [82] C. Pettersson, P. Szakálos, R. Pettersson. Influence of liquid lead and lead-bismuth eutectic on three alumina forming austenitic (AFA) steels through slow strain rate testing [J]. *J. Nucl. Mater.*, 603(2025) 155415.
- [83] S.I. Priol, J. B. Vogt. Mechanical behavior in liquid lead of Al₂O₃ coated

- 15-15Ti steel and an alumina-forming austenitic steel designed to mitigate their corrosion [J]. Eng. Fail. Anal., 2022, 139: 106443.
- [84] X. Gong, Z. Yang, Y. Deng, J. Xiao, H. Wang, Z. Yu, Y. Yin. Creep failure of a lead-bismuth eutectic at 550 and solution-annealed 15-15Ti steel exposed to stagnant 600 °C[J]. Mater. Sci. Eng. A 798 (2020) 140230
- [85] O. I. Yas' kiv, V. M. Fedirko, I. S. Kukhar. Effect of Lead and Lead-Bismuth Eutectic Melts on the Fatigue Life of Steels of the Martensitic and Austenitic Classes[J]. Mater. Sci. 50(1)(2014)102-108.
- [86] J. Ding, J. Tan, Z. Zhang. Low cycle fatigue behavior of 316LN stainless steel hollow specimen in air and liquid lead-bismuth eutectic[J]. Int. J. Fatigue 175(2023)107812.
- [87] D. Kalkhof, M. Grosse. Influence of PbBi environment on the low-cycle fatigue behavior of SNS target container materials[J]. J. Nucl. Mater., 318(2003) 143-150.
- [88] P. Marmy, X. Gong. LIMETS 3, a novel system for high strain fatigue testing in lead-bismuth eutectic[J]. J. Nucl. Mater., 450(1-3)(2014)256-261.
- [89] M. Chocholousek, E. Stergar, X. Gong, P. Marmy, S. Gavrillov, F. Ersoy. Mechanical/microstructural characteristics of environmentally-assisted degradation effects of steels in lead alloys and assessment of environmental degradation effects on performance of structural and functional components of MYRRHA ADS & LFR. MatISSE -D5.42, 2017.
- [90] B. Xue, J. Tan, X. Wu, Z. Zhang, W. Ke. Unveiling liquid Pb-Bi embrittlement of 316LN through multiscale advanced fatigue crack propagation tests steel under stainless characterization[J]. Corros. Sci. 246 (2025) 112752
- J. Luo, H. Cheng, K.M. Asl. The role of a bilayer interfacial phase on liquid metal embrittlement[J]. Science, 333(2011)1730-1733.
- [91] Z.Yu, Q. Gao, D. Yin, Y. Zhang, N. Zhou, S. . Gregory, M. Widom, J. Luo, M. P. Harmer. Segregation-induced ordered superstructures at general grain boundaries in a nickel-bismuth alloy[J]. Science 358(2017) 97-101.
- [92] G. Duscher, M.F. Chisholm, U. Alber, M. Ruhle. Bismuth-induced embrittlement of copper grain boundaries[J]. Nat Mater, 3(2004)621-626.

Note: Figure translations are in progress. See original paper for figures.

Source: ChinaXiv –Machine translation. Verify with original.